Research
Robotics—Review

Magnetic Helical Micro- and Nanorobots: Toward Their Biomedical Applications

Famin Qiu and Bradley J. Nelson*

ABSTRACT Magnetic helical micro- and nanorobots can perform 3D navigation in various liquids with a sub-micrometer precision under low-strength rotating magnetic fields (< 10 mT). Since magnetic fields with low strengths are harmless to cells and tissues, magnetic helical micro/nanorobots are promising tools for biomedical applications, such as minimally invasive surgery, cell manipulation and analysis, and targeted therapy. This review provides general information on magnetic helical micro/nanorobots, including their fabrication, motion control, and further functionalization for biomedical applications.

1 Introduction

Mobile micro- and nanorobots show great potential for applications in various fields due to their small size and mobility. In biological and medical fields, they are promising tools for minimally invasive surgery, cell manipulation and analysis, and targeted therapy [1]. In environmental fields, they have potential for use in decontamination and toxicity screening under conditions too dangerous or too small for humans to access [2]. In microfluidics, they can be used for the manipulation and transportation of micro-objects and chemicals in lab-on-a-chip devices [3].

1.1 Swimming at low Reynolds number

When the size of a robot decreases to the microscale (10^{-6} m) or nanoscale (10^{-9} m), inertial forces become negligible and drag forces from the liquid dominate. Different actuation methods for making micro/nanorobots movable in liquid must be used than the propulsive methods of larger robots. In fluid mechanics, the Reynolds number (Re) is commonly used to characterize the conditions of flow in a fluid. Re is a dimensionless quantity defining the ratio of inertial forces to viscous forces when an object moves in a fluid (Eq. (1)).

$$Re = \frac{uL\rho}{\eta} \sim \frac{F_{\text{inertial}}}{F_{\text{viscous}}} \tag{1}$$

where u and L are the speed of motion and the characteristic length of the object, respectively; while ρ and η are the density and the viscosity of the flow, respectively.

At low Re, we are in a world that is very viscous, very slow, or very small [4]. Mobile micro/nanorobots, like most microorganisms, swim in a low Re regime of less than 10^{-4}. At low Re, the flow is effectively reversible; consequently, reciprocal motion, or body motion that goes back and forth between two configurations, results in negligible net movement. In his 1977 paper "Life at Low Reynolds Number," Purcell pointed out that a non-reciprocal motion is required for a net displacement in low-Re environments, and proposed his "scallop theorem" [5]. This theorem can be understood using a theoretical three-link swimmer (Figure 1). The two hinges on this structure offer two degrees of freedom (DOF) and the structure, therefore, can move in a series of angle configurations. In Figure 1(a), a net displacement can be generated after one cycle when the swimmer moves in the series of configurations ABCDA, as this is a non-reciprocal motion. In Figure 1(b), however, the series of configurations ABCBA is reciprocal and there is no net displacement after one cycle [3]. Purcell's "scallop theorem" gives the basic requirements for design-
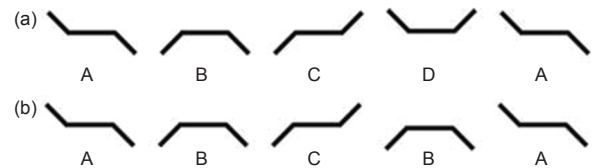
Figure 1. The two-hinged swimmer presented by Purcell. (a) A net displacement is generated when the swimmer moves in the series of configurations ABCDA after one cycle; (b) the series of configurations ABCBA is reciprocal and there is no net displacement after one cycle. (Reproduced with permission from Ref. [3])

Institute of Robotics and Intelligent Systems (IRIS), ETH Zurich, Zurich CH-8092, Switzerland
* Correspondence author. E-mail: bnelson@ethz.ch

ing micro/nanoscale swimmers: They must move in a non-reciprocal motion to achieve a net displacement.

1.2 Bio-inspired approach

Nature has inspired scientists and engineers to build many useful machines. At the microscopic scale, researchers gained ideas from motile microorganisms to create mobile micro/nanomachines. In the late 1800s, researchers established that all motile microorganisms use either flagella or cilia for motion generation. In 1973, the biologist H. Berg showed that microorganisms such as *Escherichia coli* (*E. coli*) bacteria swim in various liquids by rotating their helical flagella in a helical wave using molecular motors (Figure 2) [6].
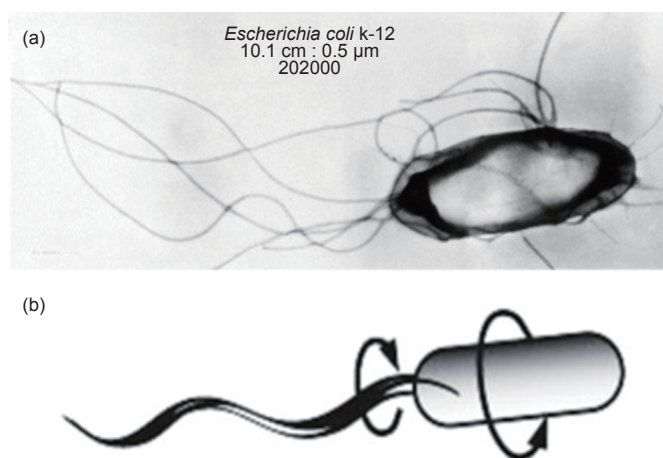

Figure 2. *E. coli* bacteria and how they swim. (a) Optical image of an *E. coli* bacteria [7]; (b) *E. coli* bacteria swim by rotating their flagella in a helical wave [8]. (Reused with permission from Refs. [7, 8])

Inspired by *E. coli* bacteria, researchers invented magnetic micro/nanorobots with helical shapes. Under a rotating magnetic field, these machines can translate a rotational motion into a translational movement to propel themselves in liquid. They have the ability to perform 3D navigation in low-*Re* environments under low-strength rotating magnetic fields (< 10 mT). Magnetic helical micro/nanorobots combine the advantages of both magnetic actuation and helical propulsion. Since magnetic fields with low strengths are harmless to cells and tissues, magnetic helical micro/nanorobots have been proposed as one of the most promising tools for biomedical applications, especially for *in vivo* applications [4, 9, 10].

1.3 History of magnetic helical micro/nanorobots

In 1996, Honda et al. proposed a helical-type swimming mechanism for microrobots in low-*Re* environments, and fabricated the first prototype of a magnetic helical robot on a centimeter (cm) scale. The swimmer consisted of a SmCo magnet (1 mm × 1 mm × 1 mm) attached to a Cu helical wire (Figure 3(a)). The cm-scale model was wirelessly actuated by an external rotating magnetic field and proved its ability to swim in low-*Re* fluids by swimming in a highly viscous silicon oil [11]. In 2005, the same group developed a similar helical robot on a smaller scale. The total length of the robot was reduced to 5.55 mm. This mm-scale helical robot was able to trail a wire and change the motion direction of the wire in a

narrow fluidic channel. It was proposed that helical microbots have great potential for navigating medical catheters in blood vessels [12].
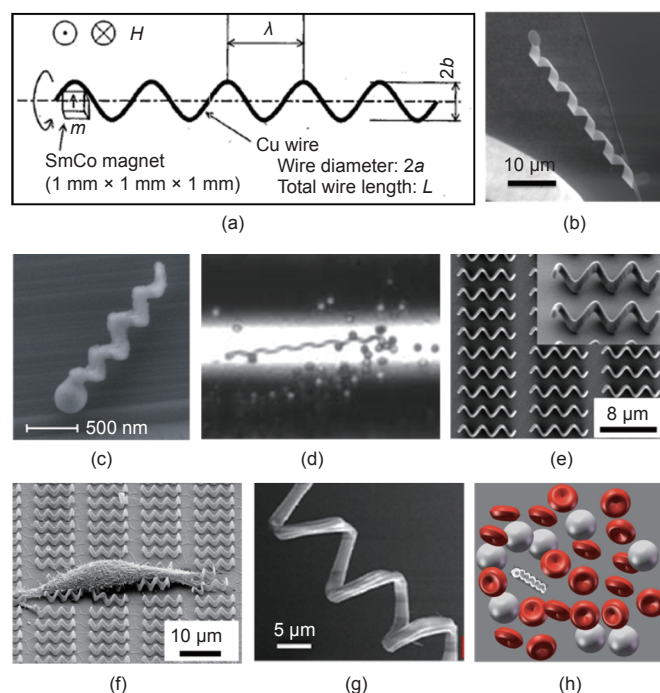
Figure 3. Magnetic helical micro/nanorobots. (a) The first prototype of a magnetic helical robot on a cm scale, reused with permission from Ref. [11] (1996); (b) the first microscale prototype of a magnetic helical robot, adapted with permission from Ref. [13] (2007); (c) the first nanoscale helical propeller, reprinted with permission from Ref. [14] (2009); (d) fluidic manipulation, adapted with permission from Ref. [3] (2010); (e) magnetic helical microrobots made by 3D laser lithography (DLW), adapted with permission from Ref. [15] (2012); (f) magnetic helical microrobots shown to be non-toxic to cells (2012); (g) helical microstructures derived from spiral vessels of plants, adapted with permission from Ref. [16] (2014); (h) nanohelix swimming in blood, reprinted with permission from Ref. [17] (2014).

In 2007, the first microscale prototype magnetic helical robot, the artificial bacterial flagellum (ABF), was invented at ETH Zurich. This microswimmer has a soft magnetic "head" and a helical "tail" with a diameter of 3 μm and a length of 30–40 μm (Figure 3(b)) [13]. The magnetic actuation and swimming behaviors of ABFs were then characterized in distilled (DI) water [18]. In 2009, the first nanoscale magnetic helical robot was fabricated using glancing angle deposition (Figure 3(c)). The nano-propellers could navigate in water under rotating magnetic fields [14]. The manipulation of micro-objects using ABFs in liquid was demonstrated (Figure 3(d)) [3].

In 2012, a new fabrication process, direct laser writing (DLW), was used to fabricate ABFs (Figure 3(e)) [15]. A helical microswimmer with a claw was able to transport microbeads in 3D [15]. The swimming performance of ABFs in heterogeneous viscous environments instead of pure water was studied [19]. These ABFs were shown to be non-toxic to mouse muscle cells within three days (Figure 3(f)) [20].

In 2013, researchers fabricated magnetic helical microstructures derived from spiral xylem vessels of plants (Figure 3(g)). This fabrication process was simple and cost-effective for mass-production [16]. In 2014, a large-scale fabrication of magnetic helical nanoswimmers by a template electrosynthesis method was presented [21]. Recently, nano-propel-

lers showed the possibility of actuation in viscoelastic media [22] and in human blood (Figure 3(h)) [17].

2 Fabrication of magnetic helical micro/nanorobots

A magnetic helical micro/nanorobot consists of at least two components, a helical body and a magnetic material. The helical body mimics the helical propulsion motion of bacterial flagella and provides the structure with the ability to perform translational movement when it rotates along the helical axis. The magnetic material enables the structure to rotate by following external rotating magnetic fields. Here, the reported fabrication methods of magnetic helical micro/nanostructures are summarized into four categories: the rolled-up method; glancing angle deposition (GLAD) method; direct laser writing method; and template-assisted method (Figure 4).
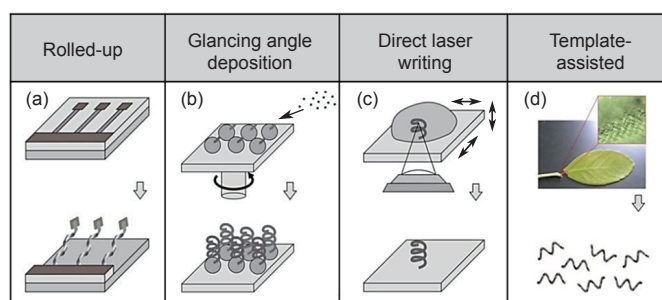
Figure 4. Fabrication of magnetic helical micro/nanorobots. (a) Rolled-up method; (b) glancing angle deposition method; (c) direct laser writing method, with parts (a–c) adapted with permission from Ref. [9]; (d) template-assisted method, adapted with permission from Ref. [16].

Rolled-up method: In 2007, the first microscale magnetic helical robot, the artificial bacterial flagellum (ABF), was fabricated by the rolled-up method (Figure 4(a)), also known as self-scrolling technology [13]. The ABF had a total length of 30 μm to 40 μm and consisted of a helical "tail" made from semiconductor materials (InGaAs) and a magnetic Ni "head" (Figure 3(b)). The fabrication was based on traditional thin film deposition methods and mono-crystalline thin film growth. By controlling the deposition parameters, such as the film thickness, the ribbon width, or the orientation of the ribbon with respect to the crystalline structure of the metal, the curvature of the ribbon could be finely tuned. By connecting these self-scrolled helical structures with a Ni plate, ABFs with diameters of around 3 μm and variable lengths of 10 μm to 100 μm were achieved. Soft materials, such as lipid bilayers, were also rolled up to form helical microstructures. Magnetic helical lipid microstructures were fabricated by electroless plating of rolled-up helical lipid microstructures with a magnetic material, CoNiReP [23].

Glancing angle deposition method: In 2009, Ghosh et al. demonstrated a batch fabrication of helical nanoswimmers by glancing angle deposition (GLAD) [14]. Spherical seeds were densely packed on a substrate, and nano-pillars were deposited at an oblique angle. By continuous rotation of the substrate, the pillars grew into a helical shape (Figure 4(b)). These helices had a diameter of 200 nm to 300 nm and a length of 1 μm to 2 μm (Figure 3(c)). The magnetic material

Co was then deposited on one side of the nanohelices along the whole body.

Direct laser writing method: In 2012, Tottori et al. developed a method to make ABFs from polymers by direct laser writing (DLW) and electron beam deposition [15]. DLW is a 3D laser lithography method that allows the creation of arbitrary 3D microstructures. A photosensitive resist was deposited on a glass substrate, which can be moved in 3D with a piezoelectric stage. Laser beams were focused into the resist and two-photon polymerization (TPP) occurred at the focal point of the laser [24]. By moving the focal point in a helical path, a helical microstructure remained after removal of the undeveloped photoresist (Figure 4(c)). Next, magnetic materials were deposited by electron beam evaporation on the entire helical structure, as shown in Figure 3(e). Other researchers have fabricated magnetic helical microstructures with magnetic nanoparticles inside the polymer instead of coating the surface of the polymer [25], and magnetic helical microstructures with hybrid materials, CoNi "heads" and polymer poly(pyrrole) "tails," have been fabricated [26].

Template-assisted method: In 2013, Gao et al. demonstrated a method to fabricate helical microswimmers using vascular plants as helical templates [16]. Various vascular plants have spiral xylem vessels. The diameters of these helical structures vary from 10 μm to over 60 μm. The helical microstructures were isolated from vascular plants, and the structures were then coated with Ni/Ti bilayers. The microstructures were cut into short helices of a few turns (Figure 4(d) and Figure 3(g)). The geometries of the swimmers can be controlled by the intrinsic structures of different plants. This is a cost-effective method that allows for mass production [16]. In 2014, the same group presented another template-assisted method to mass-produce nanosized magnetic helices [21]. Porous anodic aluminum oxide (AAO) membranes with pore sizes of 100 nm to 400 nm were used as templates. Pd/Cu nanorods were deposited into the nano-pores of the templates by electro-deposition. The Pd helical nanoswimmers were fabricated by the removal of Cu and the addition of a magnetic Ni layer.

3 Motion control of magnetic helical micro/nanorobots

Magnetic helical micro/nanorobots can perform 3D navigation under rotating magnetic fields. In this section, we use ABFs made by the DLW method (Figure 3(e)) to explain the 3D motion control of magnetic helical micro/nanorobots. The ABFs have a polymeric helical body coated with a Ni/Ti bilayer.

3.1 Magnetic actuation of ABFs
The basic principle of magnetic actuation is the movement of a magnetic object by the application of a magnetic force and/or magnetic torque. When an external magnetic field is applied to a magnetic object, the magnetic force F_M and the magnetic torque T_M acting on the body are given by Eqs. (2) and (3).

$$F_M = \vartheta(M \cdot \nabla)B \qquad (2)$$

$$T_M = \vartheta M \times B \qquad (3)$$

where ϑ is the magnetic volume of the object; B is the mag-

netic flux density; and **M** is the magnetization of the object under the magnetic field **B**. In a hard magnetic material, the magnetization of the object is independent of the applied field **B**. In a soft magnetic material, the magnitude of the vector **M** is dependent on the **B** field and the direction of **M** depends on the geometry of the object.

The ABF was coated with the soft magnetic material Ni. When an ABF is exposed to a uniform **B**, where the gradient ∇**B** is zero, the soft magnetic ABF is magnetized by the **B** field. The torque T_M drives the ABF and aligns it immediately to the **B** field. Once the direction of **M** and **B** is the same, the torque T_M becomes zero and the ABF maintains the alignment as long as **B** is unchanged. An ABF is placed in an XYZ 3D coordinate frame (Figure 5(a)), and we assume the **M** of the ABF to be perpendicular to the long axis of the ABF once it is under a **B** field. When a uniform **B** field is applied, in which the direction of **B** is minus X (Figure 5(a)), only a torque T_M (Eq. (3)) is generated. The torque brings **M** to align with **B** and vanishes. Figure 5(b) and (c) show the ABF alignment on the XY plane and XZ plane. When the direction of **B** rotates a number of degrees to B_1 on the XZ plane (Figure 5(c)), a new torque is generated, and the ABF again aligns with the B_1 field, which makes the ABF rotate a number of degrees along its long axis (Y direction in Figure 5(a)). When the **B** field is continuously rotated in a circle on the XZ plane, the ABF rotates around its helical axis continuously. A net displacement is generated when a helix rotates, which generates a translational movement to make the ABF move forward. When the rotating axis of the **B** changes its direction on the XY plane (Figure 5(b)), the direction of ABF movement changes accordingly on the horizontal plane. When the rotating axis of **B** field changes its direction on the YZ plane, the ABF swims out of the horizontal plane, which enables 3D movement of the ABF. In short, an ABF moves forward in a rotating magnetic field **B**. By simply changing the rotational axis of the **B** field, we can steer the ABF in 3D wirelessly. Helmholtz coil setup [3] is usually used to generate rotating magnetic fields for the actuation of magnetic helical micro/nanorobots.
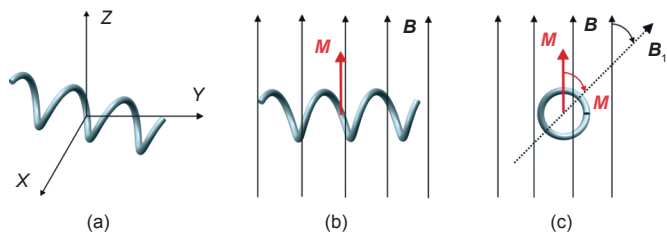
Figure 5. Motion control of an ABF under a uniform rotating magnetic field. (a) An ABF in an XYZ coordinate system. The alignment of an ABF exposed to a **B** field on (b) the XY plane and (c) the XZ plane.

3.2 Swimming behavior of ABFs

Figure 6 shows the swimming velocities of an ABF as a function of rotating frequency (f) of the external magnetic fields at a magnetic strength of 3 mT. The ABFs were 16 μm in length and 5 μm in diameter, and were made from IP-L photoresist by DLW with Ni/Ti (50 nm/5 nm) coating. The experiments were conducted in DI water, and the ABF swam
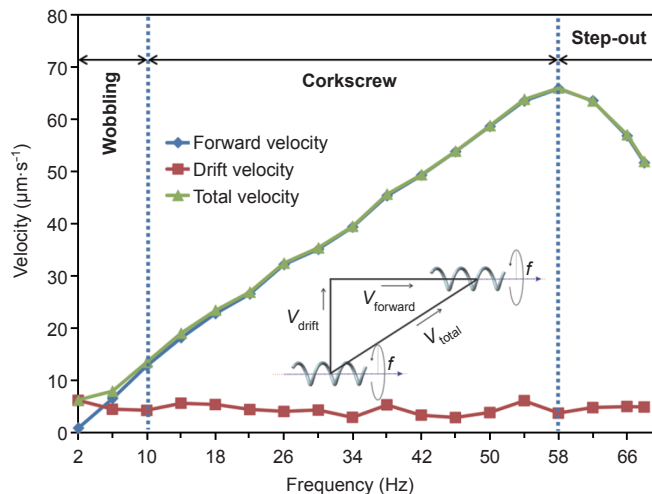
Figure 6. Swimming behavior of ABFs. The swimming plot can be divided into three regions: wobbling, corkscrew, and step-out regions. The insert shows the forward velocity ($V_{forward}$), drift velocity (V_{drift}), and total velocity (V_{total}).

on a clean and polished silicon (Si) wafer.

The ABFs show frequency-dependent swimming behavior and the swimming plot can be divided into three regions: the wobbling, corkscrew, and step-out regions (Figure 6). In the wobbling region, the ABF is actuated at a low frequency ($f < 10$ Hz) and wobbles around the helical axis while moving forward. When the frequency increases, the ABF swims in a stable corkscrew motion without wobbling, and the swimming velocity increases linearly until it reaches the maximum. The input frequency, at which the ABF reaches its maximum speed, is called the step-out frequency. When the frequency increases further, the ABF motion is in the step-out region. In this region, the velocity decreases dramatically while the frequency increases. Since the ABFs rotate near a surface due to the surface effect, they also have a drift speed perpendicular to the helical axis. The total velocity of the ABF is the sum of the forward velocity and the drift velocity (Figure 6). Drift velocity is always present if the ABFs move near a surface. In the stable corkscrew region and in some part of the step-out region, the drifting velocity is negligible compared to the increased forward velocity. A plot of forward velocity overlays the plot of total velocity in Figure 6.

4 Functionalization of magnetic helical microrobots for biomedical applications

Magnetic helical micro/nanorobots have been used to manipulate or transport micro and even smaller objects in closed or open fluidic environments by direct pushing [15, 27] and by non-contact methods (agitating the peripheral liquid when an ABF is rotating) [3]. However, for biomedical applications such as drug delivery and wireless sensing, further surface bio-functionalization with specific chemicals, such as drug molecules, is required. Qiu et al. successfully functionalized ABFs with three types of lipid-based nanoscale drug carriers (dipalmitoyl phosphatidylcholine (DPPC)-based liposomes [28], DOTAP/DOPE liposomes [29], and lipoplexes [30]). These functionalized ABFs (*f*-ABFs) were able to perform wireless single-cell targeting under low-strength magnetic fields

(< 10 mT) (Figure 7(a)). The ABFs functionalized with temperature-sensitive DPPC-based liposomes showed the ability to load both hydrophilic and hydrophobic drugs, and to trigger-release calcein (a drug model) by increasing temperature. The results showed that calcein was quickly released at 39 °C, and the release efficiency of calcein reached 73% ± 15% at 41 °C (Figure 7(b)) [28]. The ABFs functionalized with the cationic liposomes DOTAP/DOPE were able to deliver the hydrophilic model drug calcein to mouse muscle cells *in vitro* by direct contact with cells [29]. Recently, the ABFs functionalized with lipoplexes loaded with DNA showed the ability to conduct targeted gene delivery to human embryonic kidney (HEK 293) cells *in vitro*. The cells in contact with *f*-ABFs were successfully transfected by the carried DNA and expressed the encoding Venus protein (Figure 7(c)) [30]. Recent results showed the possibility of *in vivo* tracking and magnetic steering of ABFs in a mouse body [31].
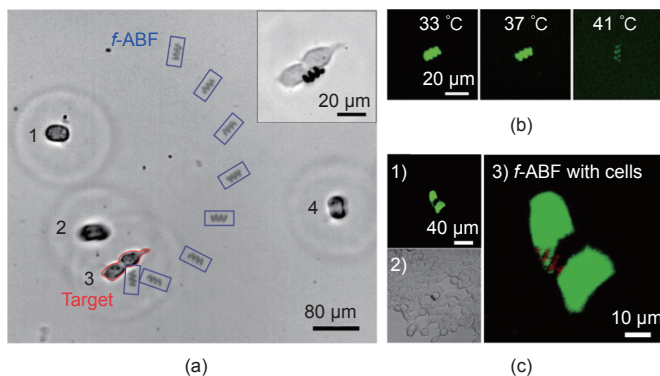
Figure 7. Functionalized ABFs (*f*-ABFs) for targeted delivery. (a) Single-cell targeting, reprinted with permission from Ref. [30]; (b) calcein release from DPPC/MSPC (1-myristoyl-2-stearoyl-*sn*-glycero-3-phosphocholine) functionalized ABFs, adapted from Ref. [28] with permission from Elsevier; (c) *f*-ABFs for targeted gene delivery, 1) the fluorescent image, 2) the transmission image, 3) a zoomed overlay of two images, adapted with permission from Ref. [30].

5 Summary and future outlook

Inspired by the flagellar propulsive motion of bacteria such as *E. coli*, magnetic helical micro/nanorobots can perform controlled, sub-micrometer precision and 3D navigation in low-*Re* environments under low-strength rotating magnetic fields (< 10 mT). They are promising tools for biomedical applications, such as minimally invasive surgery, cell manipulation and analysis, and targeted therapy. Several challenges remain before realizing their biomedical application.

First, the *in vitro* and *in vivo* biocompatibility of magnetic helical micro/nanorobots should be investigated. Additionally, after they complete their task *in vivo*, the challenge remains of how best to remove micro/nanorobots from the human body. One way is to guide them to an area and remove them by minimally invasive surgery. The best solution may be to make them biodegradable or bio-absorbable, so new biocompatible and biodegradable materials, such as biodegradable hydrogels, are needed to achieve this.

Second, in biological and medical environments, the physiological fluids are more complex than DI water and contain various proteins and macromolecules. In order to conduct

biomedical applications, further functionalization of magnetic helical micro/nanorobots is needed to improve their movement in these heterogeneous viscous environments.

Finally, magnetic helical micro/nanorobots are controlled and tuned by changing the magnetic fields manually. Automatic control should be integrated to facilitate the control of these devices. In future, multiple micro/nanorobots working in a collaborative way should be explored for complex tasks.

Compliance with ethics guidelines

Famin Qiu and Bradley J. Nelson declare that they have no conflict of interest or financial conflicts to disclose.

References

1. B. J. Nelson, I. K. Kaliakatsos, J. J. Abbott. Microrobots for minimally invasive medicine. *Annu. Rev. Biomed. Eng.*, 2010, 12(1): 55–85
2. W. Gao, J. Wang. The environmental impact of micro/nanomachines: A review. *ACS Nano*, 2014, 8(4): 3170–3180
3. L. Zhang, K. E. Peyer, B. J. Nelson. Artificial bacterial flagella for micromanipulation. *Lab Chip*, 2010, 10(17): 2203–2215
4. J. J. Abbott, et al. How should microrobots swim? *Int. J. Robot. Res.*, 2009, 28(11–12): 1434–1447
5. E. M. Purcell. Life at low Reynolds number. *Am. J. Phys.*, 1977, 45(1): 3–11
6. H. C. Berg, R. A. Anderson. Bacteria swim by rotating their flagellar filaments. *Nature*, 1973, 245(5425): 380–382
7. T. Baba, et al. Construction of *Escherichia coli* K-12 in-frame, single-gene knockout mutants: The Keio collection. *Mol. Syst. Biol.* 2006, 2(1): 2006.0008
8. W. R. DiLuzio, et al. *Escherichia coli* swim on the right-hand side. *Nature*, 2005, 435(7046): 1271–1274
9. K. E. Peyer, S. Tottori, F. Qiu, L. Zhang, B. J. Nelson. Magnetic helical micromachines. *Chemi. Eur. J.*, 2013, 19(1): 28–38
10. K. E. Peyer, L. Zhang, B. J. Nelson. Bio-inspired magnetic swimming microrobots for biomedical applications. *Nanoscale*, 2013, 5(4): 1259–1272
11. T. Honda, K. I. Arai, K. Ishiyama. Micro swimming mechanisms propelled by external magnetic fields. *IEEE Trans. Magn.*, 1996, 32(5): 5085–5087
12. K. Kikuchi, A. Yamazaki, M. Sendoh, K. Ishiyama, K. I. Arai. Fabrication of a spiral type magnetic micromachine for trailing a wire. *IEEE Trans. Magn.*, 2005, 41(10): 4012–4014
13. D. J. Bell, S. Leutenegger, K. M. Hammar, L. X. Dong, B. J. Nelson. Flagella-like propulsion for microrobots using a nanocoil and a rotating electromagnetic field. In: *Proceedings of IEEE International Conference on Robotics and Automation*, 2007: 1128–1133
14. A. Ghosh, P. Fischer. Controlled propulsion of artificial magnetic nanostructured propellers. *Nano Lett.*, 2009, 9(6): 2243–2245
15. S. Tottori, L. Zhang, F. Qiu, K. K. Krawczyk, A. Franco-Obregón, B. J. Nelson. Magnetic helical micromachines: Fabrication, controlled swimming, and cargo transport. *Adv. Mater.*, 2012, 24(6): 811–816
16. W. Gao, et al. Bioinspired helical microswimmers based on vascular plants. *Nano Lett.*, 2014, 14(1): 305–310
17. P. L. Venugopalan, R. Sai, Y. Chandorkar, B. Basu, S. Shivashankar, A. Ghosh. Conformal cytocompatible ferrite coatings facilitate the realization of a nanovoyager in human blood. *Nano Lett.*, 2014, 14(4): 1968–1975
18. L. Zhang, et al. Characterizing the swimming properties of artificial bacterial flagella. *Nano Lett.*, 2009, 9(10): 3663–3667
19. B. J. Nelson, K. E. Peyer. Micro- and nanorobots swimming in heterogeneous liquids. *ACS Nano*, 2014, 8(9): 8718–8724

20. F. Qiu, et al. Noncytotoxic artificial bacterial flagella fabricated from biocompatible ORMOCOMP and iron coating. *J. Mater. Chem. B*, 2014, 2(4): 357–362

21. J. Li, et al. Template electrosynthesis of tailored-made helical nanoswimmers. *Nanoscale*, 2014, 6(16): 9415–9420

22. D. Schamel, et al. Nanopropellers and their actuation in complex viscoelastic media. *ACS Nano*, 2014, 8(9): 8794–8801

23. S. Schuerle, S. Pané, E. Pellicer, J. Sort, M. D. Baró, B. J. Nelson. Helical and tubular lipid microstructures that are electroless-coated with CoNiReP for wireless magnetic manipulation. *Small*, 2012, 8(10): 1498–1502

24. S. Kawata, H. B. Sun, T. Tanaka, K. Takada. Finer features for functional microdevices—Micromachines can be created with higher resolution using two-photon absorption. *Nature*, 2001, 412(6848): 697–698

25. M. Suter, et al. Superparamagnetic microrobots: Fabrication by two-photon polymerization and biocompatibility. *Biomed. Microdevices*, 2013, 15(6): 997–1003

26. M. A. Zeeshan, et al. Hybrid helical magnetic microrobots obtained by 3D template-assisted electrodeposition. *Small*, 2014, 10(7): 1284–1288

27. T. Y. Huang, et al. Cooperative manipulation and transport of microobjects using multiple helical microcarriers. *RSC Adv.*, 2014, 4(51): 26771–26776

28. F. Qiu, R. Mhanna, L. Zhang, Y. Ding, S. Fujita, B. J. Nelson. Artificial bacterial flagella functionalized with temperature-sensitive liposomes for controlled release. *Sens. Actuators B Chem.*, 2014, 196: 676–681

29. R. Mhanna, et al. Artificial bacterial flagella for remote-controlled targeted single-cell drug delivery. *Small*, 2014, 10(10): 1953–1957

30. F. Qiu, S. Fujita, R. Mhanna, L. Zhang, B. R. Simona, B. J. Nelson. Magnetic helical microswimmers functionalized with lipoplexes for targeted gene delivery. *Adv. Funct. Mater.*, 2015, 25(11): 1666–1671

31. A. Servant, F. Qiu, M. Mazza, K. Kostarelos, B. J. Nelson. Controlled *in vivo* swimming of a swarm of bacteria-like microrobotic flagella. *Adv. Mater.*, 2015, 27(19): 2981–2988